To the Graduate Council:

I am submitting herewith a thesis written by Thomas Ebel entitled "Analysis, Modeling, and testing of a Multi-Receiver Wireless System for Telemetry Applications." I have examined the final electronic copy of this dissertation for form and content and recommend that it be accepted in partial fulfillment of the requirements for the degree of Master of Science, with a major in Electrical Engineering.

Dr Bruce Bomar
Bruce Bomar, Major Professor

We have read this dissertation
and recommend its acceptance:

Dr Peter Solies

Dr Montgomery Smith

Acceptance for the Council:

Carolyn R Hodges
Vice Provost and Dean of the Graduate School

(Original signatures are on file with official student records.)

Analysis, Modeling and Testing of a Multi-Receiver Wireless System for Telemetry Applications

A Thesis

Presented for the

Master of Science in

Electrical Engineering

Degree

The University of Tennessee Space Institute

Thomas Ebel

August, 2007

Dedication

This thesis is dedicated to Drs John and William Ebel, who inspired me and taught me so much.

Abstract

This thesis investigates the potential value of multiple co-located receiver units for telemetry applications. In this thesis, a test board based on the NRF24L01 RF chip produced by Nordic Semiconductor was tested. Testing consisted of sending pseudo-random test data over a link between two test boards at progressive distances. Packet loss rate was identified as the dominant failure mode of the chip, and was used to determine performance increase. A parametric model of the chip performance was developed based on coherent and noncoherent FSK detectors and curve fit to the experimental data to model the performance of a single GFSK receiver with unknown parameters. The chip exhibited an estimated 10 fold improvement in bit error performance at short range, with the performance improvement dropping off as distance increased. This result implies that there may be significant utility to using multiple receiver systems when traditional methods of improving performance such as amplifiers and antennas do not provide the necessary benefit.

Table Of Contents

Chapter Page

I. Introduction....1

II. Background....3

Telemetry and Remote Sensing in General....3

Wireless Technologies....4

Specific Problems for this Thesis....6

III. Description of Hardware and Software....8

Hardware....8

Board Level Software....10

MATLAB Software....13

IV. Experimental Procedures and Collected Data....16

Configuration....16

Measurement Sequence....17

Presentation of Results....17

V. Theoretical Model of Operation....20

Determination of Parameters....20

Unification of Data....23

Determination of System Loss Factor....25

Summary of Model Parameters....25

VI. Expansion to Multiple Receivers....28

Three Receivers....28

Analysis of Short Range Effects....29

Inclusion of 2 Receiver Hybrid Case....29

Illustration of Probability Envelope and Correlation....30

VII. Summary and Conclusions....33

List of References....36

Appendix....39

Vita....43

List of Figures

Figure Page

Fig 1: Packet Format....9

Fig 2: Test Board Block Diagram....10

Fig 3: Transmitter and Receiver Program Flow....12

Fig 4: Program Flow for Packet Reconstruction....14

Fig 5: Structure of 3 Dimensional Packet Array....14

Fig 6: Block Diagram of Test Setup....16

Fig 7: Illustration of Results of Test at 0dBm Power Setting....18

Fig 8: Illustration of Results of Test at -12dBm Power Setting....19

Fig 9: Illustration of Results of Test at -18dBm Power Setting....19

Fig 10: Collected Data Assembled Onto a Common
Distance Axis Equivalent to 1mW Output Power....24

Fig 11: Coherent Receiver System Loss Factors as a Function of Distance....26

Fig 12: Noncoherent Receiver System Loss Factors as a Function of Distance....26

Fig 13: Loss Factors Determined from Distance Normalized Error Probabilities....27

Fig 14: Observed Bit Error Probabilities for 3 Receiver Composite
Case and Single Receiver Average....29

Fig 15: Triple Receiver Bit Error Probability Envelope....32

Fig 16: Two Receiver Bit Error Probability Envelope....33

Nomenclature

AES	Advanced Encryption Standard
CRC	Cyclic Redundancy Check
FCC	Federal Communications Commission
FSK	Frequency Shift Keying
FTDI	Future Technologies Devices International ltd
GF	Galois Field
GFSK	Gaussian Frequency Shift Keying
GPIO	General Purpose Input Output
I^2C	Inter-Integrated Circuit
ISM	Industrial Scientific Medical
IVTM	In-Vehicle Tire Monitoring
MAC	Media Access Controller
MSE	Mean Square Error
NSA	National Security Agency
RF	Radio Frequency
RFID	Radio-Frequency Identification
SPI	Serial Peripheral Interface
UART	Universal Asynchronous Receive and Transmit
USB	Universal Serial Bus
UTSI	University of Tennessee Space Institute
UWB	Ultra Wideband

List of Symbols

α	Noise Factor Parameter
λ	Wavelength (m)
$A_{carrier}$	Maximum Carrier Amplitude (v)
d	Transmitter-Receiver separation distance (m)
dB	Decibels
E_b	Bit Energy Received (j)
G_r	Receiver Antenna Gain
G_t	Transmitter Antenna Gain
L	System Loss Factor (not related to propagation)
m	Meters
mm	Millimeters
N_0	Noise Energy Spectral Density (w)
ppm	Parts Per Million
PL	Path Loss
P_E	Probability of Error
P_r	Power Received (w)
P_t	Power Transmitted (w)
T_{bit}	Bit Time (s)

Chapter 1: Introduction

As wireless sensing and telemetry systems become ubiquitous, more applications are being discovered. The general telemetry problem involves taking advantage of advances in the sophistication of microelectronics to take on-site measurements, and then relay the data to a remote site where the data are reduced and analyzed.

In the case of moving, rotating, or enclosed components, such as the fan blades or internal engine compartments of aircraft, or the rotor blades of helicopters, or even the wheels of automobiles, traditional wires cannot serve to extract data. This necessitates the use of a wireless solution, or local storage until the test is complete, to accomplish the necessary data collection.

In confined spaces where the physical size and weight of any sensing device must be carefully controlled to avoid interfering with the operation of the system to be tested, power consumption, board size, and component count must be minimized. To accomplish this minimization, such systems must rely on embedded, single or small-count chipset architectures. In these cases, in the sensing and transmission unit, energy consumption, physical size, and possibly other factors are all at a premium. In many applications, however, the receiver component is not as limited as the transmitter component, often having access to grid power (essentially unlimited, in terms of most embedded applications). The receiver may also have fewer restrictions in terms of board size and complexity.

All radio systems have a common problem with data loss. Multipath factors, interfering transmitters in the same band, and background noise are some of the factors that will contribute to signal corruption and degradation. The standard approach to improving the performance of a radio system is to add a gain factor to the system, in the form of improved antennas or amplifiers. However, the benefits gained from adding redundant receivers is not as well studied. This lends itself to the problem of quantifying the performance increases gained with respect to the increasing complexity of the receiver system when the transmitter complexity is held constant.

In this thesis, increasing complexity is examined with the use of three identical co

located receivers. This thesis describes the examination of a single case study of multiple receivers, with the goal of developing a model of the performance of a single chip wireless transceiver in terms of bit error rate. An RF chip was selected and a board was designed to incorporate multiple RF chips. The system was then tested by sending pseudo-random data over the RF link for effective distances ranging from 10 to 280 meters. The pseudo random data contained sufficient structure for the detection of errors and dropped packets. The error statistics were extracted from the collected data and compared to the theoretical basis for receivers of the type. This model was used to examine and quantify the performance improvement gained by using multiple redundant receivers. The dominant failure mode turned out to be packet loss as opposed to bit error contained in the delivered packets, with the improvement most significant at short distances.

Chapter 2 describes the available technologies for telemetry and describes in more detail the specific problems to be addressed in this thesis, as well as discussing the rationale for selecting the specific RF chip used. Chapter 3 describes the hardware and software used in the experimentation. Chapter 4 describes the procedures used to collect the data and presents the results, Chapter 5 discusses the development of a model for packet loss rate versus distance, expressed in terms of bit error rate; and chapter 6 expands the analysis to incorporate the effects of redundant receivers. Chapter 7 presents a summary and conclusions.

Chapter 2: Background

Section 1: Telemetry and Remote Sensing in General

Telemetry, from the Greek roots *tele*, for remote, and *metron*, for measurement, is any technology or technologies used for exactly that purpose; remote measurement. Telemetry systems can be broken down into two broad categories, wired systems and wireless systems. This thesis deals with wireless systems.

Wireless sensors are used in a tremendous number of applications. WABCO Automotive advertises their IVTM (In Vehicle Tire Monitoring) system, a remote tire pressure sensor designed to improve productivity, and reduce truck downtime by allowing trucks to self-monitor their tires, eliminating the need for costly, time consuming, and unpleasant manual checks. [1]

Michelin is developing multiple systems for tire monitoring, both for truck and automotive tires. The Etire^{tm} system consists of a rubber dock vulcanized to the inside of the tire, a passive RFID sensor, and an external reader. [2], [3]. The system is designed to provide a passive system allowing managers better inventory control and tracking, with many of the same benefits as the IVTM system.

Michelin's joint venture with TRW Automotive [4], EnTire solutions, is a battery powered system similar to that of the IVTM system for passenger cars and light trucks. As with all three of the tire products, the system is intended as an after market add on to any tire system, since any tire system can benefit from such remote sensing technology.

In the industrial controls sector, Sensicast advertises "...a complete, wireless sensor network built for industrial and commercial environments where wireless operation and high reliability are required." [5] Sensicast specializes in remote monitoring of manufacturing processes and commercial applications, including so called "smart facilities".

In aviation, the high cost of components, especially flight safety or critical components, is driving the same type of remote sensing development. A google search performed on Mar 18, 2007 with the keywords "aircraft component sensor" yielded 993,000 results. Aerospace applications can easily require components with temperature tolerances in the hundreds of degrees Celsius. These goals are naturally ambitious, as most commercial

components are only rated to 55 degrees Celsius. Even more important, traditional methods of circuit board traces, wires, or even fiber optic systems cannot work in a high-speed rotating environment. Traditional methods like slip-rings will not provide sufficient data throughput or mechanical reliability. This forces the use of wireless technologies in many applications.

Section 2: Wireless Technologies

Government funding and other private applications have driven the development of a large number of options for deploying off the shelf wireless systems. The three dominant standards available for these applications are Bluetooth, Zigbee, WLAN (Wireless-Lan). These standards operate primarily in the FCC allocated band from 2.4 to 2.5 GHz which is the most widely used ISM (Insustrial – Scientific – Medical) band for sensing and telemetry applications. An emerging technology also exists called UWB (Ultra-Wideband) .

Bluetooth [6], [7] is a standard for low speed data transmission, with data rates of up to 2 Mbit per second, over short range. Bluetooth operates in several power classes with ranges of up to 100m line of sight, and is intended as a wire-replacement technology. Bluetooth is commonly used for wireless PC peripherals such as mice and keyboards. Bluetooth is limited in its utility for sensor applications, as one master device can communicate with only one slave device at a time, and only seven slaves may be active at any one time. Additionally, with multiple devices limited to a single on-air channel, net throughput for any given device drops. Only the most recent standard of Bluetooth incorporates data encryption in the form of 128 bit AES encryption, and as such, security is a common concern of Bluetooth systems.

Zigbee [8] is another standard for low speed wireless data transmission, and competes with bluetooth. It is a standard for low speed, self organizing networks, with data transmission rates of up to 250 Kbits per second. The original development of Zigbee originated in response to the limitations of Bluetooth, and was developed with wireless sensor networks in mind, specifically applications such as home automation. Zigbee devices have low power requirements, short range, and can self organize into a network, making such networks more robust to individual elements connecting and disconnecting. Zigbee also

incorporates the AES encryption system. However, the low data rate for Zigbee limits utility in sensing applications that generate a high data rate. Also, Zigbee has a significant protocol stack complexity to ensure interoperability of large numbers of devices, increasing device complexity.

WLAN, sometimes called Wi-Fi, is essentially a wireless ethernet technology. WLAN, particularly the IEEE 802.11G specification [9], can support user throughput of up to 37 Mbit per second per channel. 11 channels are specified in the standard, with as many as three channels available for use by a single device. Many systems can boast high reliability and connectivity at ranges of 100m or more. Additionally, since WLAN is related to ethernet, and most WLAN systems have their own (MAC) Media Access Controller addresses, such systems minimize the design requirement to interface sensors to a network or the internet. Security concerns limit the use of WLAN under certain circumstances, as the WEP (Wired Equivalent Privacy) protocol is notoriously easy to hack. WLAN architecture networks must be strictly configured and maintained in order to meet the minimum requirements for processing official US Government data, and cannot be configured for the transmission of classified data. [10] Additionally, while WLAN systems have become quite small, even being implemented as single-chip solutions, the power requirements for many systems remains above the 1000 mW level, limiting utility in locations where systems must rely on stored power for long periods of time.

UWB [11] is a set of related, emerging technologies that spread the transmitted signal out across a large portion of the radio spectrum. The FCC defines UWB as any system with a fractional energy bandwidth of 0.25 or greater, or any system with a bandwidth of 500 MHz or more. UWB systems are often pulse based, but spread-spectrum technologies also fall into this category. The IEEE 802.15.4a draft standard is an under-development standard for pulse-based wireless systems. UWB offers the possibility of incredibly high data rates, such as the Freescale Semiconductor XS110 chipset, advertise transmission bit rates in excess of 100 Mbit per second. However, UWB chipsets are still in development, and no mature standards exist for interoperability.

Finally, a number of non-standardized systems operate in the 2.4 GHz ISM band. Such devices lack the interoperability of devices that adhere to a particular standard, but gain

a reduction of complexity as a result. Chipcon, a division of Texas Instruments, Cypress Semiconductor, Freescale Semiconductor, Nordic Semiconductor, and a number of other manufacturers offer such systems. Typically, such systems offer comparable range and data rate to Bluetooth and Zigbee devices. In many cases, use of a single chip or chipset solution allows the system developer to select only the desired features for a particular application, and this can be provided at a significant savings in terms of size and power requirements, among others. However, higher level security functions such as NSA suite-B [12] encryption protocols are not available on any single chip solution as of this writing.

In the case of the system board used in this thesis, the NRF24L01 [13] transceiver chip developed by Nordic Semiconductor was employed. The NRF24L01 has an extremely small package size, 4x4 mm, as well as a high on air data rate of 2 Mbps and a low current consumption of 12 mA. The chip also communicates over an SPI bus, allowing for simple control and configuration without requiring significant processor overhead. This reduced the requirements of the microcontroller.

Section 3: Specific Problems for This Thesis

Within the scope of designing a wireless system to suit a specific application's needs, is the situation where the wireless system component need not be symmetric. All of the low-cost, low-power embedded solutions discussed earlier have been symmetric systems; that is to say, the transmitter component is the same as the receiver component. This is advantageous from a system design perspective in that a single circuit board design or module can serve as both the transmitter and the receiver element, improving economies of scale and simplifying the system design process.

However, situations arise when a performance increase is desired without changing pre-engineered hardware. In these cases, required performance increase must be achieved by repetition; using multiple receivers on a single channel, increasing the probability of data being received successfully. In some environments, such as environments with severe degradation do to large amounts of metal structure, such as internal to an engine assembly, positioning of receiver elements becomes a deciding factor in reception.

The research for this thesis used an existing test board to test and quantify the performance increase of using multiple receivers compared to a single receiver for this specific technology. The test board was based around three NRF24L01 transceivers that operate in the 2.4 GHz ISM band. An analysis of the reception results yielded a model for the system performance and the type of performance increases that may be achieved. This is discussed in the context of other standards for measuring performance increase and any advantages of this system are highlighted. Additionally, any special considerations for using this particular technology are discussed. The next chapter describes in detail the hardware and software running on the specific test board used for the experimentation for this thesis.

RF chip performance is measured in terms of two data failure modes: packet loss and corrupted bits within each packet. It was initially expected that the second error mode would be the dominant error mode, and data collection was designed to detect and measure this. Specifically, the software designed for the transmitter and receiver boards was optimized to correct multiple errors in the received data. The transmitter and receiver boards were non-synchronous; the only method of communication between them was the RF link to be tested. Therefore a robust method of simulating real (pseudo-random) data had to be devised that also allowed for packet synchronization and reconstruction, and allowed for detection of dropped packets. To accomplish this, a prime number pseudo-random number generator was implemented, and is described in more detail in chapter 3. The generator produced a deterministic sequence of numbers, allowing for correction of errors in received data as well as detection of dropped packets.

After the experiment had been conducted, it was observed that the first error mode, packet loss, was the dominant form of failure; specifically, many more packets were observed to be missed by one or more receivers than packets received with bit errors in the payload section. The details of the experimentation and the data collected are described in chapter 4. The analysis subsequently focused on modeling this packet loss rate and determining bit error characteristics from this. Only dropped packets were considered for the analysis section. Since it was found that the packets received with errors in the data had a negligible effect on the overall performance of the system.

Chapter 3: Description of Hardware and Software

Section 1: Board Hardware

The primary components used were the ADUC7024 microcontroller [14] and the NRF24L01 RF chip [13]. The ADUC7024 is an ARM7 variant produced by Analog Devices. It has available 40 GPIO pins, overlapping with a a UART and a multi purpose serial port multiplexer, capable of emulating a UART, SPI, or I^2C interface. The maximum clock rate for the ADUC7024 is 41.78 MHz, based on an internal phased locked loop increasing a 32 KHz digital watch crystal by a factor of 1275. Available on the ADUC7024 are two 12 bit DAC modules and a high bandwidth 12 bit ADC capable of 1 MSPS with a maximum clock rate. This particular controller was chosen in part to allow for testing using the on board ADC directly. One of the DAC units is connected to a ± 14 ppm voltage controlled crystal oscillator on the third RF module for the purpose of testing the effects of clock variation on error rate. That test is not a part of this thesis.

The test board consisted of a single ADUC7024 microcontroller linked to three NRF24L01 units over a shared SPI bus. A block diagram showing the board signals is provided Fig 1. The NRF24L01 was selected because it offered a high degree of integration, small package size, and high data rate. The NRF20L01 operates in the 2.4 GHz ISM band, with a channel spacing in 1 MHz steps. It has an on-air transmission rate of up to 2 Mb/s, with a listed sensitivity of -82 dBm at a 0.1% bit error rate. The NRF24L01 is packet based, differentiating between 256 bit payloads by RF channel, as well as a 24, 32, or 40 bit packet address. An 8 or 16 bit CRC (Cyclic Redundancy Check) function is also available. Each packet is constructed of three parts, as shown in figure 1. These parts are an 8 bit preamble, a 24 bit address, and a payload of 32 bytes. A 24 bit address and a maximum size payload were used for the tests in this thesis. This set of options was selected to maximize throughput. The NRF24L01 has overhead between transmitted packets, requiring maximum payload length and minimum address length for maximum throughput.

8 Bit Preamble	24 Bit Address	256 Bit Payload

Fig 1: Packet Format

The ADUC7024 was run at an internal clock speed of 41.78 Mhz, multiplied up from a 32 Khz watch crystal. Connection to the PC was made using one of two FTDI USB interface chips, one FT245R USB2 to parallel chip [15], and one FT232R USB to serial chip [16]. Both are single chip solutions that implement a 128 byte FIFO and handle all physical and link layer requirements for connection to a USB2 bus.

The FT245R was connected to two of the GPIO ports of the ADUC7024, one for the 8 bit parallel data, and the second for the control lines. The microcontroller was capable of transmitting 180 kilobytes per second via the FT245R, however, the virtual COM port drivers were limited to the maximum COM port speed of 921.6 Kb/s, which limited the maximum throughput to the PC. The FT232R was linked to the ADUC7024 UART, and achieved a similar throughput to the FT245R. For all of the tests the PC was connected to the FT245R.

The SPI enable lines were connected to three General Purpose Input Output (GPIO) pins on the ADUC7024 to handle the shared SPI bus. To improve the data throughput, the SPI clock divider value was set to 0x03, which resulted in an SPI clock rate of 5.8 Mhz. This performance parameter was in excess of the maximum suggested by the ADUC7024 datasheet [14], compared to a published upper limit on the clock rate of 3.482 Mhz, however no performance degradation was observed when operating at this frequency. Fig 2 illustrates the hardware block diagram for the test board.

All communication and configuration of the NRF24L01 modules was handled through the SPI bus. The NRF24L01 modules were completely reconfigured whenever a mode change occurred to ensure that the behavior was absolutely repeatable and predictable.

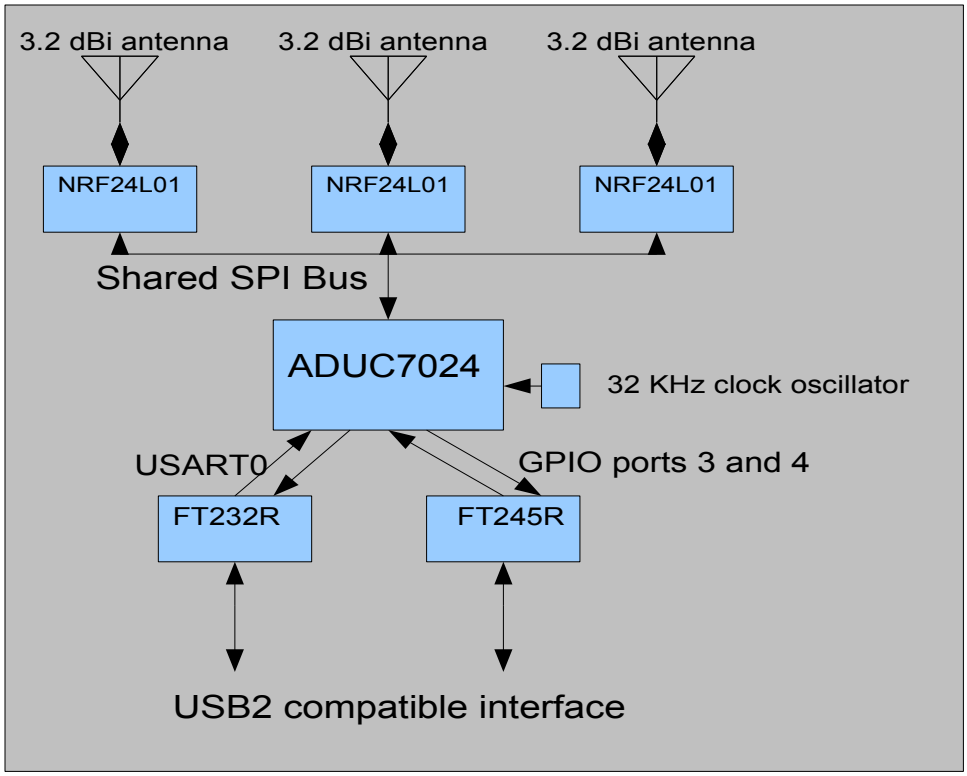

Fig 2: Test Board Block Diagram

Section 2: Board Level Software

Two separate boards were used in all tests, one operating as a transmitter, and one as a receiver. This allowed the receiver board to collect data from all three RF chips in real time. No connection was available between the transmitter and receiver boards, so no synchronization was performed. The software run on the board depended on whether the board ran in transmitter mode or receiver mode. In transmitter mode, the data payloads were assigned values based on the Galois field GF65521, and multiplicatively incremented with the generator element 65448. This was done to ensure a pseudo random sequence of bits transmitted in the payload, while retaining a level of recovery at the PC end. The packet payload was divided into 16 elements, each element containing a 16 bit word that conformed to:

$$E_{i+1} = (E_i * 65448) \, modulo \, 65521 \quad (1)$$

Each packet is a continuation of the sequence in the previous packet. This structure

serves two purposes. First, it creates a pseudo-random data sequence intended to mimic real data being transmitted, rather than with a sequence of identical packets. Second, the structure of the data allowed for detection of missed packets, as the packet elements served as sequence numbers. Finally, the structure of the data, as explained in the next section, allowed for robust correction of a minimum of 14 bit errors, and detection of a minimum of 15. This corresponds to the effective error tolerance of a linear block code with (n, k) of (256, 227). [17] However, the simple reconstruction algorithm obviated the need to design a linear decoder, simplifying the problem significantly.

In order to ensure that the receiver had sufficient delay to poll all three RF chips on the receiver board, between each packet transmitted, an incremental counting loop of 0x25000 was used to insert delay. The available packet CRC was not used, since redundancy and error checking was built into the data. This loop continued until a stop command was issued from the PC or power was removed.

On the receiver end, a simple polling scheme was used to recover the packets. Using the shared SPI bus, each receiver was polled in turn to see if a packet had been received. If a packet was received, it was extracted and dumped to the PC for storage and analysis. If no packet was received, the next receiver was polled. This loop continued indefinitely until a stop command was issued from the PC, or power was removed.

The PC collected the data dumped from the receiver board over a USB2 connection into Hyperterm, using a COM port emulator provided by FTDI ltd. The data was sent to the PC in a human readable format and stored as a plain text file. Since the receiver and the transmitter were not synchronized, nor was Hyperterm, incomplete packets transmitted from the receiver board had to be stripped by hand using a text editor. These were startup and shutdown effects caused by the conclusion of a Hyperterm session while still in the process of reporting a packet. Once the data had been collected and stored on the PC hard disk, subsequent offline analysis was performed in MATLAB. Board level program flow is illustrated in fig 3.

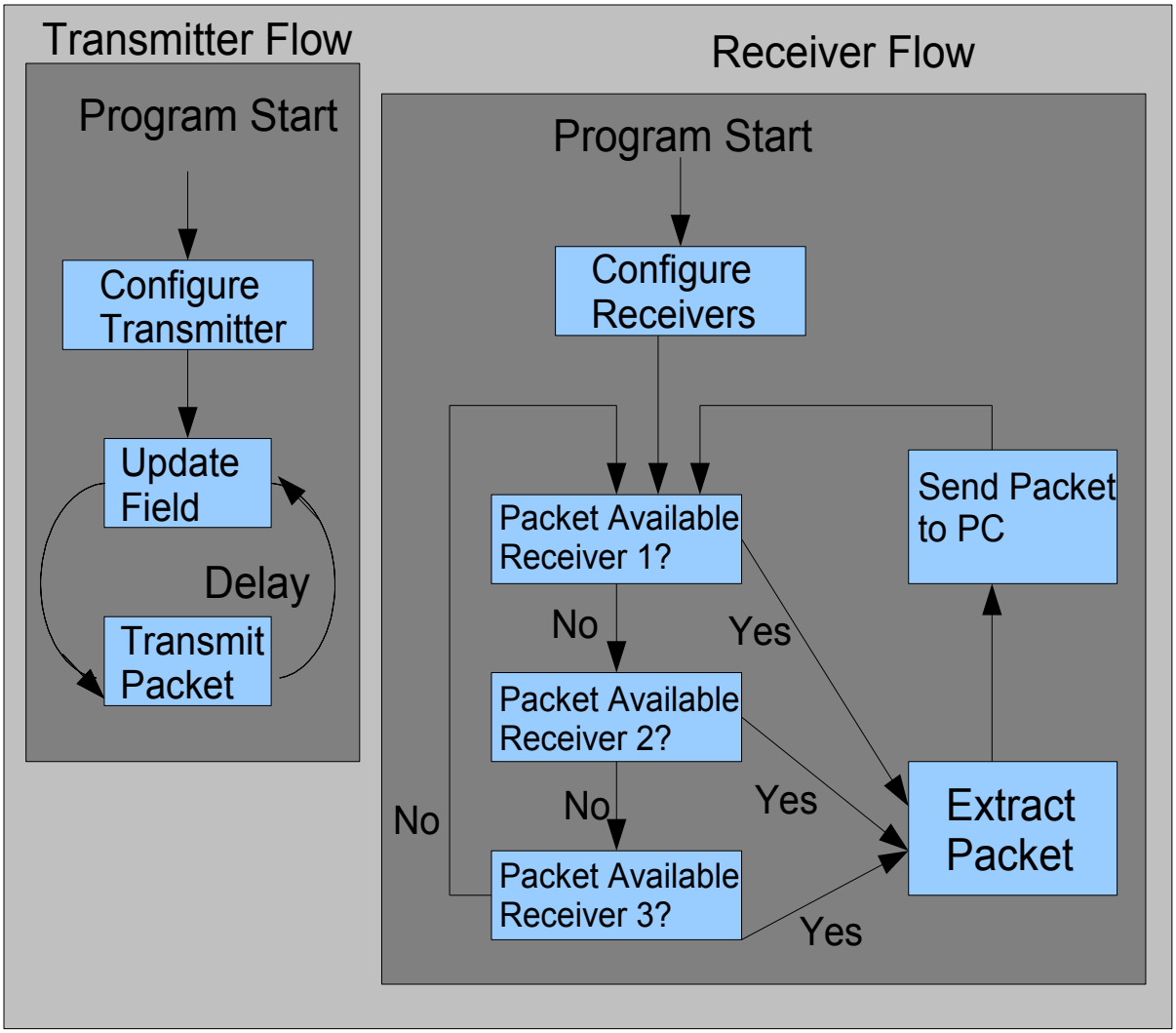

Fig 3: Transmitter and Receiver Program Flow

Section 3: MATLAB Software

Data analysis was performed in MATLAB. Since no synchronization occurred between the transmitter board and the receiver board, the MATLAB software was designed to recover the transmitted data. First, the human readable text files were parsed into an array, each entry containing 17 fields. The first field represented the receiver number. The following 16 fields represented the 16 bit payload elements.

Packet reconstruction and sorting followed. Reconstruction, as illustrated in Fig 4, involved traversing through the array of received packets, and reconstructing each packet individually. Each packet is constructed based on a deterministic sequence; the next element in the sequence is found by:

$$E_{(i+1)} = (E_i * 65448) \, modulo \, 65521 \tag{2}$$

And the previous element in the sequence is:

$$E_{(i-1)} = (E_i) * (\frac{1}{65448}) \, modulo \, 65521 = (E_i) * 37697 \, modulo \, 65521 \tag{3}$$

Because of this structure, any packet can be reconstructed from any of the 16 elements within the packet. Determination of the most likely packet transmitted, for a given received packet occurred by first creating a set of 16 possible packet reconstructions, based on the elements of the received packet. Each of those possible reconstructions is compared with the actual received packet; the reconstruction with the most matching elements is assumed to be the packet that was actually transmitted. Once the set of 'idealized packets' was created, the packets were sorted so they could be analyzed.

Sorting consisted of assigning the packets to a three dimensional array sorted by receiver number, illustrated in Fig 5. This was performed using the idealized packets for each received array element to be sorted. Since not all packets were received by all three receivers (referred to as dropped packets), some of the array elements were all zeros. Positions in the array filled with zeros represented packets missed by a given receiver. Bit by bit voting across all three packets returns the 'decisioned packet'. Error counts are achieved by a bit by bit comparison with the idealized packets. By examining the transition between first element of a packet and the last element of a previous packet, packets missed by all three receivers could be identified.

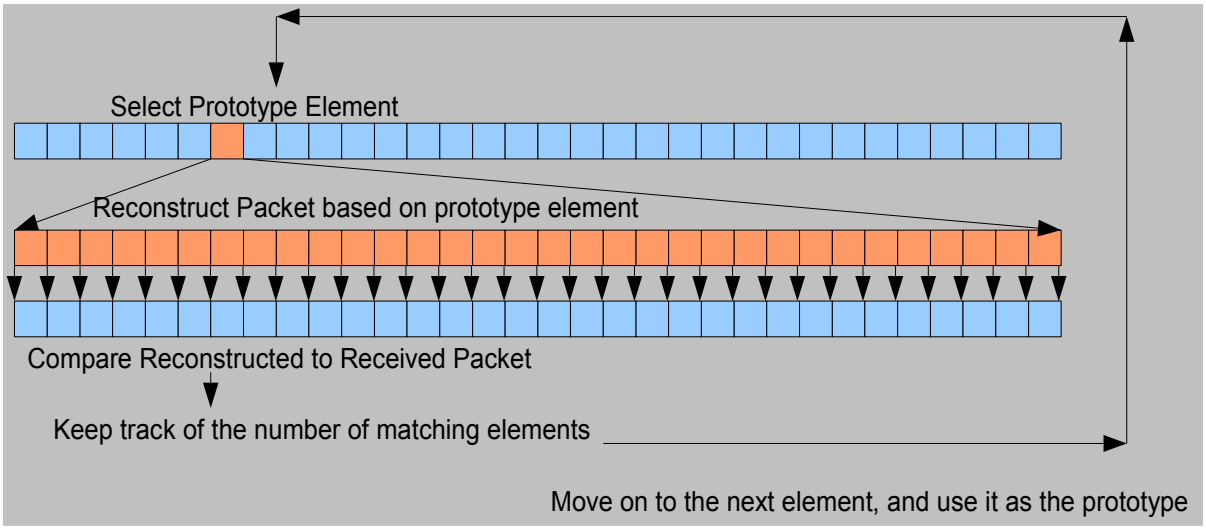

Fig 4: Program Flow for Packet Reconstruction

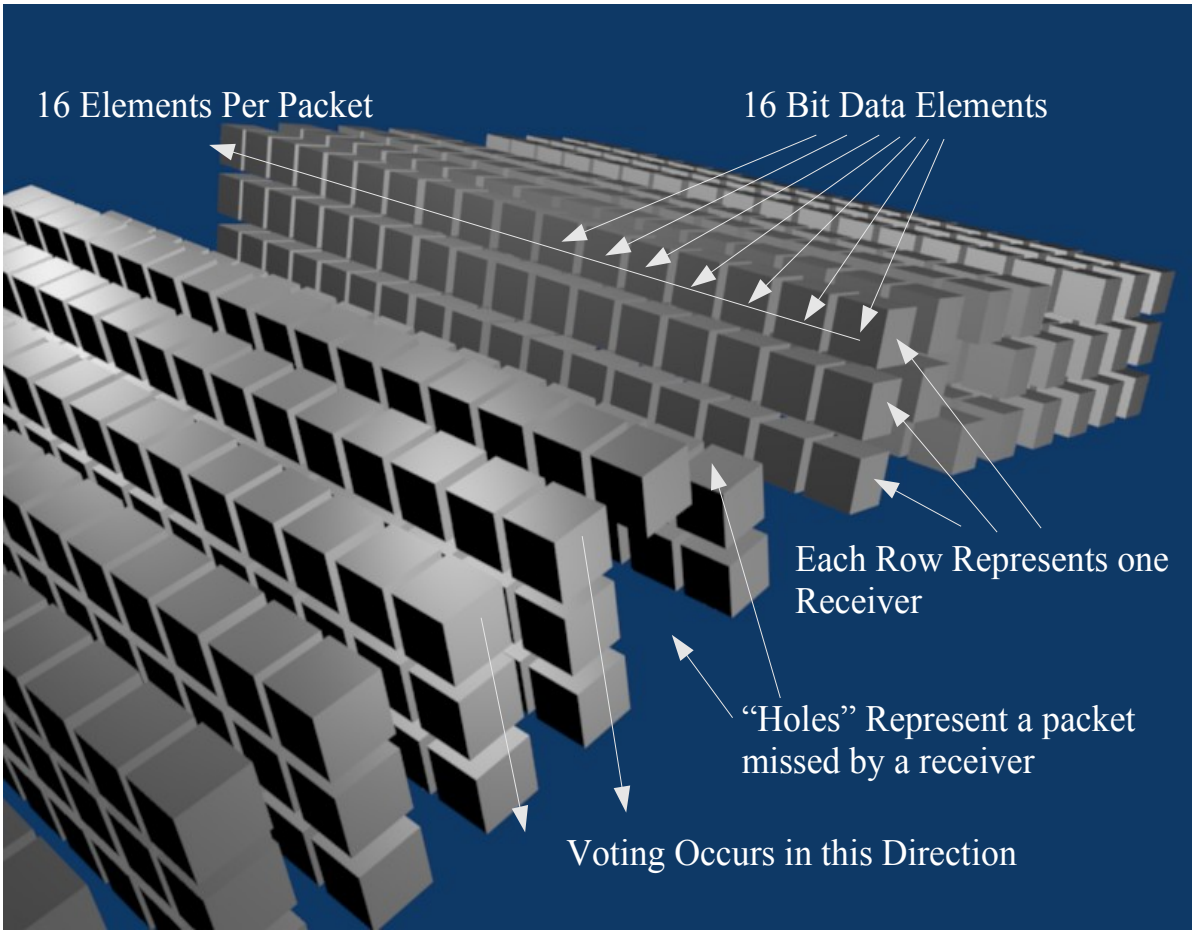

Fig 5: Structure of 3 Dimensional Packet Array

Once the packets had been sorted, the packets were examined to look for gaps in the enumerated sequence, to identify situations where all three receivers had missed a transmitted packet. This provided a total count of packets received by each receiver, as well as a total count of all packets transmitted. Once this was known, error statistics could be computed from the collected data.

While intended to ensure a high degree of redundancy in the data, as bit errors were expected to be distributed sparsely but evenly throughout the received data, the packet error rate proved much higher than the bit error rate.

Analysis of the data required bit error rates as opposed to packet error rates. Since packet error overwhelmingly dominated in-payload bit error, the packet error rate had to be converted into a bit error rate [18]. In the operational mode for these tests, the NRF24L01 transmits a preamble for synchronous decoding of 8 bits, followed by a 24 bit address. This leads to a header length of 32 bits, an error in any one of which will cause a packet to be dropped. To convert from packet error to bit error probability therefore, can be accomplished by treating the packet header as a Bernoulli process [20] and inverting Bernoulli trial formulation:

$$P_{packet\,received\,successfully} = (1 - P_{bit\,error})^{32} \tag{4}$$

to get:

$$P_{bit\,error} = 1 - \sqrt[32]{\frac{N_{possible\,receptions}}{N_{successful\,receptions}}} \tag{5}$$

Once bit error probabilities were known for all test points, analysis to model the performance of the transmitter/receiver pairs could be performed. It should be noted at this point that since this is a sampling of a stochastic process, all bit error probabilities are an estimate of the actual bit error probabilities.

Chapter 4: Experimental Procedures and Collected Data

Section 1: Configuration of Equipment

This section describes the physical experimental procedures used to measure the packet error rate for the NRF24L01 test board. Previous tests not described in this thesis demonstrated what appeared to be a trend that a 24 bit address, with the CRC turned off provided the maximum throughput. For the tests examined in this thesis, the address was configured to the default address of 0xE7E7E7. For all tests, the CRC was turned off to support bit error detection.

Both boards were held 0.5m off the ground by a plastic box. The receiver was connected to the PC by a USB cable, providing both power and data download, and control. The transmitter board was battery powered, and continuously transmitted throughout the test. All transmitter-receiver distances are in reference to the central antenna. The next section goes into detail about the steps taken for each data point collected. The test construct is illustrated in Fig 6.

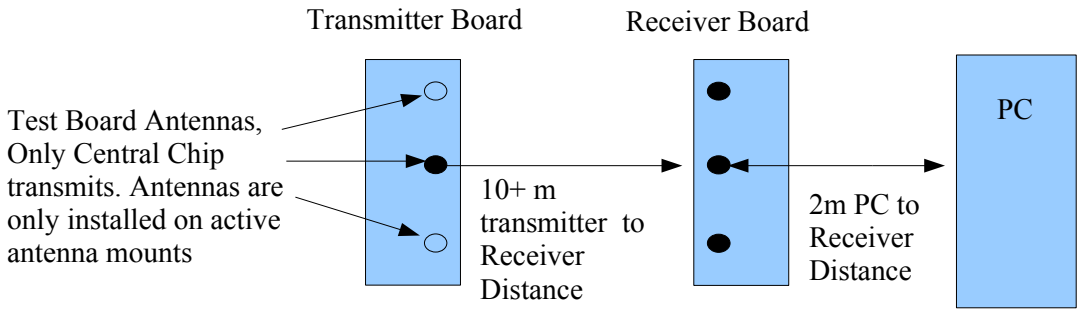

Fig 6: Block Diagram of Test Setup

Section 2: Measurement Sequence

1) For the data point associated with each distance, the line formed by the antennas on the transmitter board was aligned with the corresponding line on the receiver board to within 10°. The central antenna to central antenna distance was used as the reference distance, and is set to the measurement distance for that data point.

2) The PC confirmed that the link to the receiver board is active, then the PC began data acquisition from the receiver board. The PC collected data for 20 minutes or until 10,000 kB of data were collected, whichever took longer. This corresponds to approximately 80,000 data points.

3) The PC shut down data collection from the receiver board, and the transmitter board was moved to the location for the next test, returning to step 1.

The next section details the actual data points collected during this test. Uneven terrain at UTSI limits tests to 40m or less of test distance, before elevation changes greater than 0.25m occur, limiting the distance before which collected data become suspect due to terrain obstruction [20] and other terrain scattering effects. To combat this, multiple test runs were taken at variable transmitter power settings.

Section 3: Presentation of Results

The overwhelming error mode for the NRF24L01 was the dropped packet, with a dropped packet defined as the situation when a receiver failed to report a packet reception, rather than an error within the payload. Supported by a communication from Nordic, the analysis was performed on the dropped packet rate.

In the figures below, denoted 7, 8, and 9, the collected data are presented. The actual values are presented in the appendix; the total sample space represents the total number of

packets sent by the transmitter during each test, reconstructed from the received sequence. The packets missed by all receivers column represents the number of instances where all three receivers failed to report the reception of the same packet. These are reconstructed from gaps in the enumerated sequence (as described in chapter 3). The total missed packets incidents column represents the total number of situations where a receiver failed to report the reception of a transmitted packet, and provides an estimate of the averaged performance of the individual receivers.

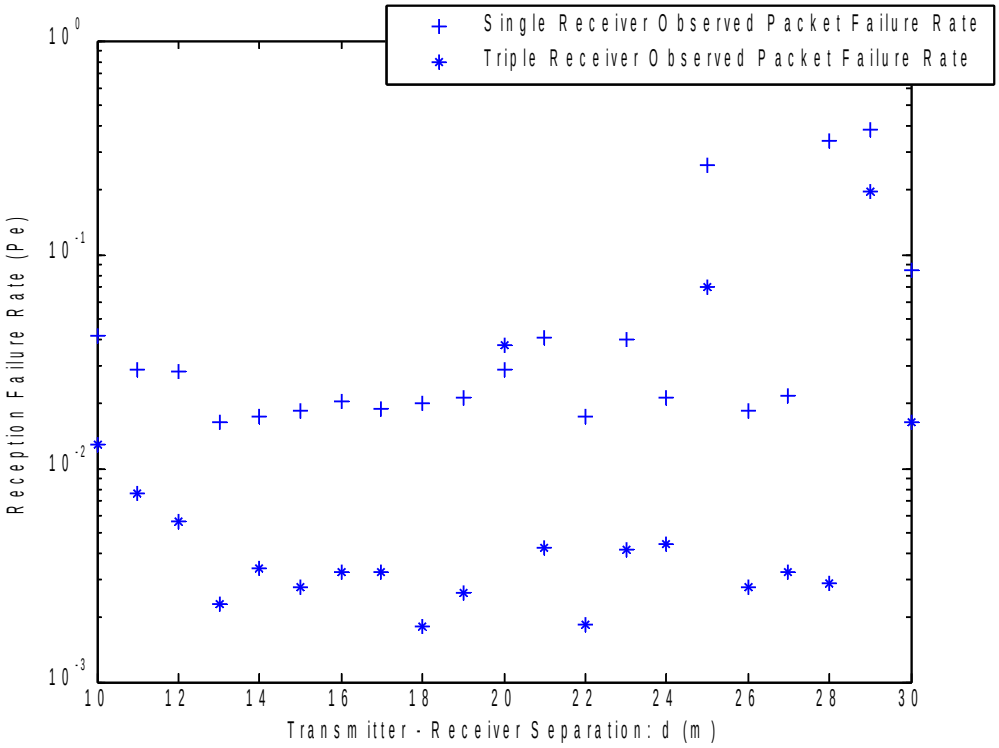

Fig 7: Illustration of Results of Test at 0dBm Power Setting

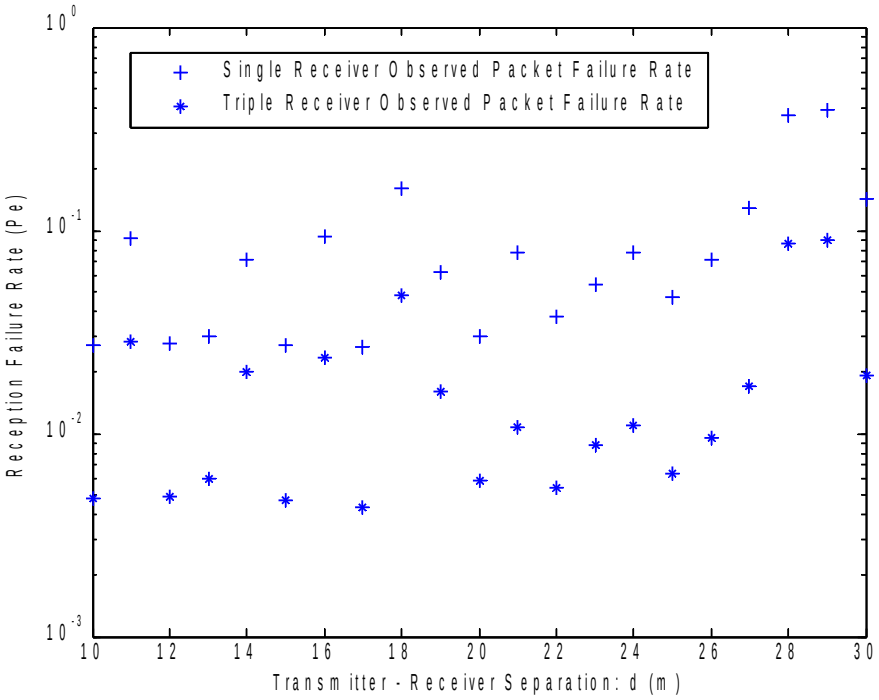

Fig 8: Illustration of Results of Test at -12dBm Power Setting

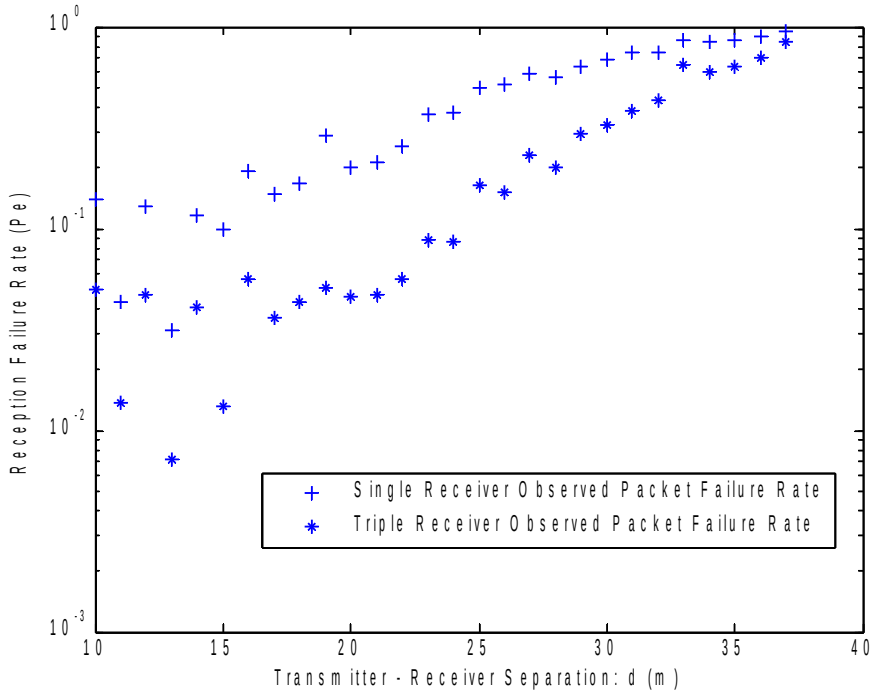

Fig 9: Illustration of Results of Test at 0dBm Power Setting

Chapter 5: Theoretical Model of Operation

Section 1: Determination of Parameters

To verify the analysis performed on the NRF24L01 test board, it is necessary to have a model of the system performance to compare with the experimental results. This section presents a model that was developed to evaluate the expected performance of the test board, that was then be used as a guide for the analysis of the experimental data.

Two constructs are used to describe the data analyzed in this section. The first construct is the average single receiver case. For this case, the results of each receiver were collected independently, and a ratio of successfully received packets to transmitted packets was computed for each distance measurement. The average of these measurements for each distance measurement at a particular power setting was taken, as an ensemble average. The three receiver composite case, or simply the three receiver case, was treating all three receivers working in tandem as a single composite receiver. In this case, if any one of the three receivers successfully received a packet, it was considered to be successfully received.

The NRF24L01 is described as a GFSK (Gaussian Frequency Shift Keying) transceiver; however, not all operational parameters are defined. Since GFSK is similar to the well understood Frequency Shift Keying (FSK) transceiver, the NRF24L01 will be modeled as such.

An FSK receiver can operate one of two ways; using coherent detection, or noncoherent detection. In the case of coherent FSK detection, the probability of error is given by [20]:

$$P_{e,FSK,coherent} = Q\left(\sqrt{\frac{\alpha E_b}{N_0}}\right) = \frac{1}{(\sqrt{2\pi})} \int_{\sqrt{\frac{E_b}{N_0}}}^{\infty} e^{-y/2}\, dy \tag{6}$$

with α representing a modulation parameter, with α given by 1.0 for orthogonal FSK, 1.217 for optimal FSK, and 2.0 for continuous-phase FSK; in the case of noncoherent detection, the probability of error is given by [20]:

$$P_{e,FSK,noncoherent} = \frac{1}{2} e^{\frac{-E_b}{2N_0}} \tag{7}$$

with E_b being the average energy received per bit and N_0 representing the one sided power spectral density of the noise. The noise is assumed to be white-gaussian.

The NRF24L01 datasheet [13] has only one published error probability point. A bit error probability of 0.001 corresponds to a received signal strength at the input terminals of -82dbm. The received bit energy can be expressed as [21]:

$$E_b = \frac{1}{2} A_{carrier}^2 T_{bit} \tag{8}$$

where A is the carrier amplitude, T being the bit time. However, since the transmitter is transmitting with constant power, the energy per bit can be computed based on the output power of the transmitter, since power is energy per unit time. The expression for energy per bit becomes:

$$E_b = P_R T_{bit} \tag{9}$$

Incorporating this information into the expressions for the bit error probabilities above, yields the noise term:

$$P_{e,FSK,coherent} = 0.001 = Q\left(\sqrt{\frac{\alpha(10^{-11.2} W * 5x10^{-7} s)}{N_0}}\right) \tag{10}$$

which yields:

$$\frac{N_{0,coherent}}{\alpha} = 3.3036\,x\,10^{-19} \tag{11}$$

and

$$P_{e,FSK,noncoherent} = 0.001 = \frac{1}{2} e^{\frac{-1*(10^{-11.2} W * 5x10^{-7} s)}{2 N_0}} \tag{12}$$

yields:

$$N_{0,noncoherent} = 2.5382\,x\,10^{-19} \tag{13}$$

Free space propagation is governed by the Friis Free Space Equation [21]:

$$P_R(d) = \frac{P_t G_t G_r \lambda^2}{(4\pi)^2 d^2 L} \tag{14}$$

P_t is the nominal transmitted power, λ is the wavelength of the signal, G_t and G_r are the gains of the transmitting and receiving antennae, d is the transmitter – receiver separation, and L is

an aggregate factor for other losses.

Combining these equations yields the following expressions for the bit error probabilities of the coherent and noncoherent detection probabilities:

$$P_{e,FSK,coherent} = Q\left(\frac{\lambda}{4\pi d}\sqrt{\frac{\alpha P_T G_T G_R T_{bit}}{L N_0}}\right) \quad (15)$$

in the coherent detector case, and

$$P_{e,FSK,noncoherent} = \frac{1}{2} e^{\left(\frac{-P_t G_t G_R \lambda^2 T_{bit}}{2(4\pi)^2 d^2 L N_0}\right)} \quad (16)$$

in the noncoherent detector case.

Some of these parameters are known at the outset. At 2.4 GHz, $\lambda = 0.125$m. G_t and G_r are both a gain factor of 2. [21] Since the NRF24L01 has an on air data rate of 2 Mbps, T_{bit} is known to be 5 x 10^{-7}. Pt is 1 mw. Incorporating these terms, as well as the noise parameter computed earlier, into the previous equations yields new expressions for the bit error probabilities:

$$P_{e,FSK,coherent} = Q\left(\frac{0.125}{4\pi d}\sqrt{\frac{(10^{-3}W)*2*2*(5x10^{-7}s)}{L*(3.3036x10^{-19})}}\right) \quad (17)$$

Which yields:

$$P_{e,FSK,coherent} = Q\left(\frac{1}{32\pi d}\sqrt{\frac{6.054x10^{9}}{L}}\right) \quad (18)$$

and the second expression:

$$P_{e,FSK,noncoherent} = \frac{1}{2} e^{\left(\frac{-(10^{-3}W)*2*2*0.125^2(5*10^{-7}s)}{32(\pi)^2 d^2 L(2.5382x10^{-19})}\right)} \quad (19)$$

Which yields:

$$P_{e,FSK,noncoherent} = \frac{1}{2} e^{\left(\frac{(-3.8475x10^{6})}{\pi^2 d^2 L}\right)} \quad (20)$$

Determination of the loss factor L requires examination of the received data to determine the transmitter-receiver separation distance for which a bit error rate of 0.1% occurs. As explained in the experimental procedures chapter, the data were impractical to collect along a single distance axis, and so multiple data sets were collected with varying output power levels.

Section 2: Unification of Data

Due to limitations explained in chapter 3, the data could not be collected along a single continuous track, so three data sets with variable transmitter power were collected instead. In order to derive a meaningful PLE term, those data must first be unified onto a single distance axis. The derivation begins with the Friis Free Space Equation as presented in the previous section:

$$P_R(d) = P_t \frac{G_t G_r \lambda^2}{(4\,pi)^2 L} d^{-2} \tag{21}$$

Since all terms in this equation except d^{-2} are constant, those constants can be grouped into a single parameter K:

$$P_R(d) = K\, d^{-2} \tag{22}$$

To convert between power scales requires applying a scaling factor to d. This can be conceptually understood as follows: A transmitter in free space operating at 1W at a distance X from a receiving station will have the same amount of energy delivered to the receiving station if it were operating at 4W and a distance of 2X from the receiver. Solving the above for d:

$$d = \left(\frac{P_r}{K}\right)^{-\frac{1}{2}} \tag{23}$$

This yields an expression for distance as a function of received power. If the power is increased by a factor of R, making the new transmitted power expression:

$$P'_t = R\, P_t \tag{24}$$

The received power as a function of distance becomes:

$$P_R(d) = \frac{K}{R} d^{-2} \tag{25}$$

Now the distance can be expressed as a scaling factor based only on the difference in power R.

$$R^{\left(\frac{1}{2}\right)} d = \left(\frac{P_r}{K}\right)^{-\frac{1}{2}} \tag{26}$$

Applying this to the three data sets allows them to be unified along a single axis and treated as a single data set, illustrated in Fig 6. Applying a curve fit to the unified data set

allows for the determination of the system loss factor, L, in the next section.

In an attempt to improve the fit of the data, the assumption of the log distance path model [21] can be applied:

$$PL(d) \propto \left(\frac{d}{d_0}\right)^n \tag{27}$$

where n is a parameterization value accommodating non ideal losses. Following the same pattern as above yields a variable formula for unifying the data.

$$P_R(d) = \frac{K}{R} d^{-n} \tag{28}$$

However, incorporating this additional degree of freedom to the model of receiver performance does not affect the outcome. Fig 10 illustrates the data combined onto a single distance axis:

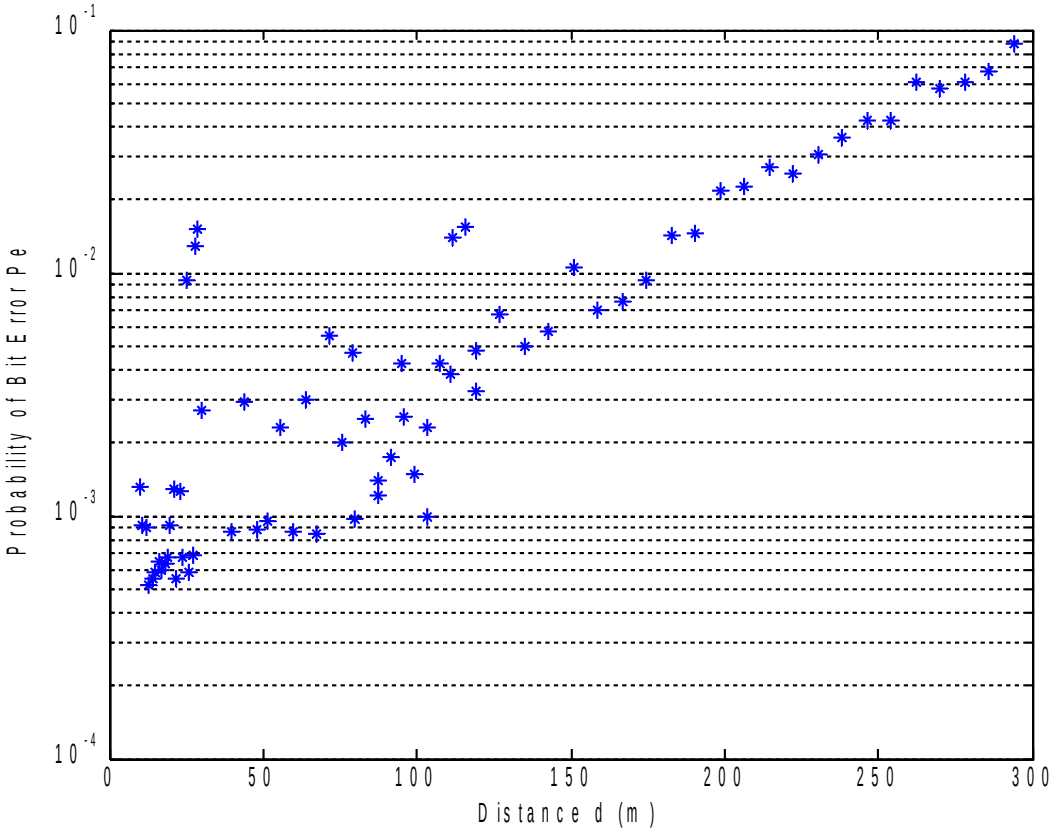

Fig 10: Collected Data Assembled Onto a Common Distance Axis Equivalent to 1mW Output Power

Section 3: Determination of System Loss Factor

From the above graph, the system loss factor L can be determined for both the coherent and noncoherent models by applying a curve fit to the experimental data. Solving (18) and (20) for L yields:

$$\frac{32*\pi*d*Q^{-1}(P^2_{e,FSK,coherent})}{(6.054\,x\,10^9)}=\frac{1}{L} \tag{29}$$

$$\frac{\pi^2 d^2*\ln(2*P_{e,FSK,noncoherent})}{(-3.8475\,x\,10^6)}=\frac{1}{L} \tag{30}$$

Using the experimental data for (29) and (30) yields experimental values for L. However, the system loss factors generated by these plots are not constant as would be expected. This approach is illustrated in Figs 11 and 12. This result is somewhat problematic, and indicative of an irreducible noise floor, or some other effect interfering with signal reception at close range, perhaps amplifier saturation.

An alternative method for determining path loss is to use (18) and (20). By varying values of L, and by minimizing the MSE (mean square error), the best fit for the L value for each model can be determined. This is illustrated in Fig 13. Furthermore, by examining the quality of fit for both models, it can be determined whether the receiver is a coherent or noncoherent detector. The coherent detector case yields a MSE of 1.6 x 10^{-3}, for a loss factor of 3.38, and the noncoherent detector case yields a MSE of 2.1 x 10^{-3}.for a loss factor of 2.55.

Section 4: Summary of Model Parameters

The previous sections in this chapter determined all of the values for he parameters in (15) and (16) from experimental data or published values. Table 1 summarizes all of the parameters for (15) and (16). The antenna gains are presented in terms of absolute magnitude, not decibels. In the case of the parametric model developed in the previous sections, only the N_0 parameters and the L parameters were determined experimentally, all others were published in hardware datasheets or determined from published values.

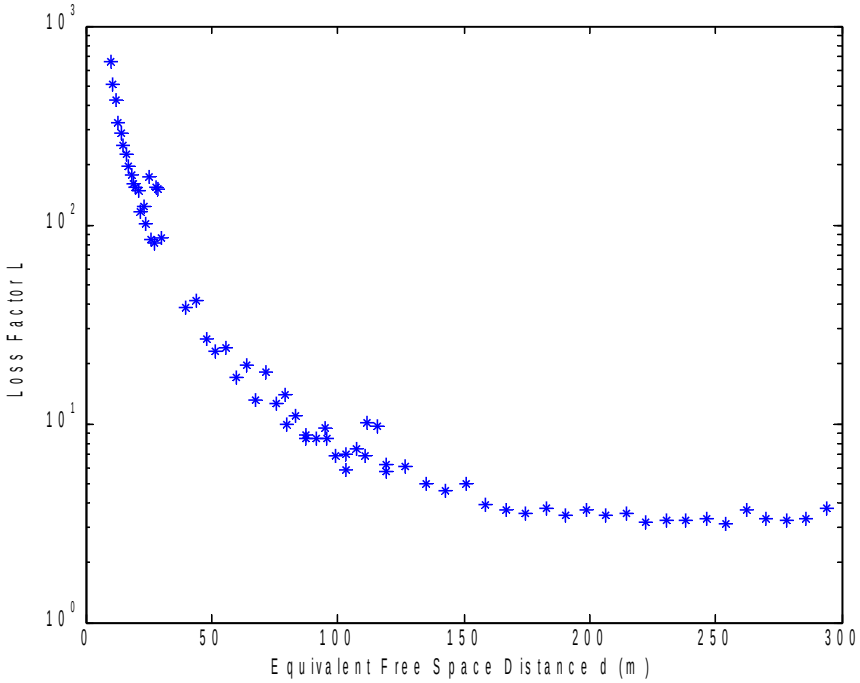

Fig 11: Coherent Receiver System Loss Factors as a Function of Distance

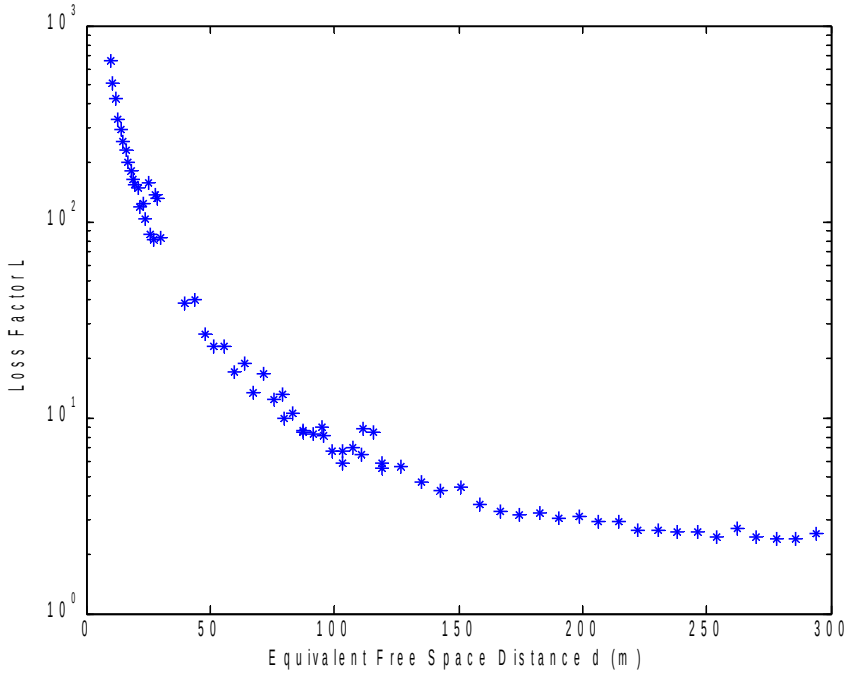

Fig 12: Noncoherent Receiver System Loss Factors as a Function of Distance

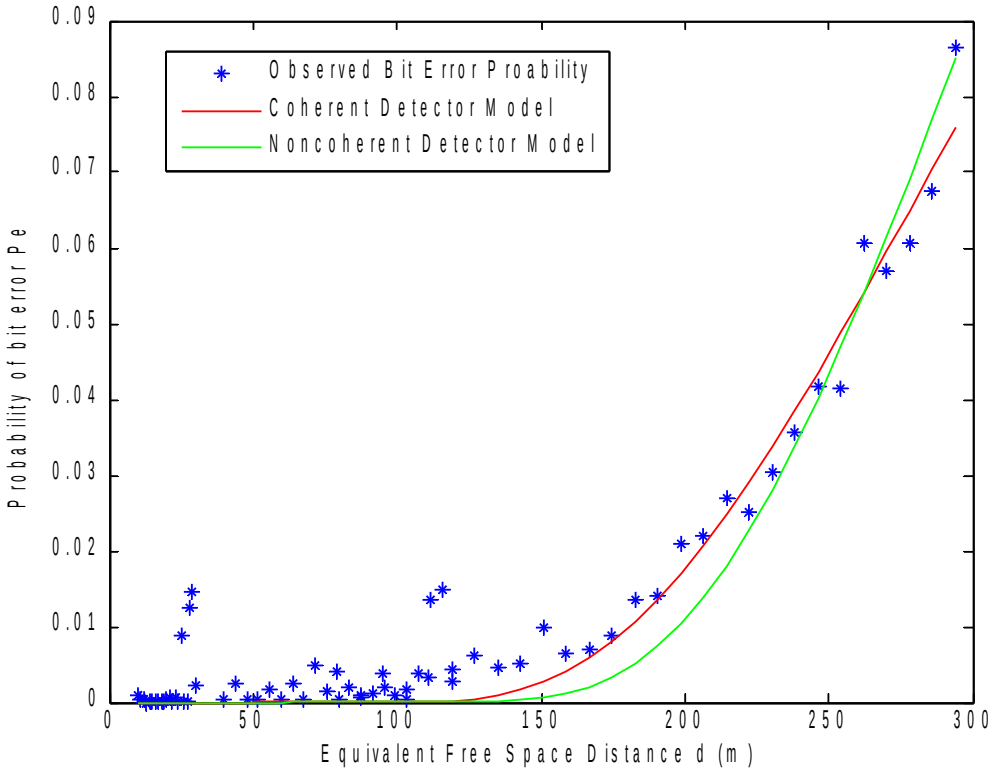

Fig 13: Loss Factors Determined from Distance Normalized Error Probabilities

Table 1: Determined or Calculated Parameters of the NRF24L01 Test Board

Parameter	Description	Value
G_t	Transmitter Antenna Gain	2
G_r	Receiver Antenna Gain	2
$L_{coherent}$	Loss Factor for Coherent Receiver Model	3.38
$L_{noncoherent}$	Loss Factor for Noncoherent Receiver Model	2.55
λ	Wavelength	0.125m
$N_{0,\ coherent}/\alpha$	Coherent Model Noise Spectral Density	3.30×10^{-19}
$N_{0,\ noncoherent}$	Noncoherent Model Noise Spectral Density	2.54×10^{-19}
T_{bit}	Bit Time	5×10^{-7} s

Chapter 6: Expansion to Multiple Receivers:

Section 1: Three Receivers

Since the receiver board contained three receivers, and the best possible performance is obtained when using all three receivers in tandem, the first logical step is to examine the performance of composite 3-chip receiver. This performance is illustrated in fig 14:

.

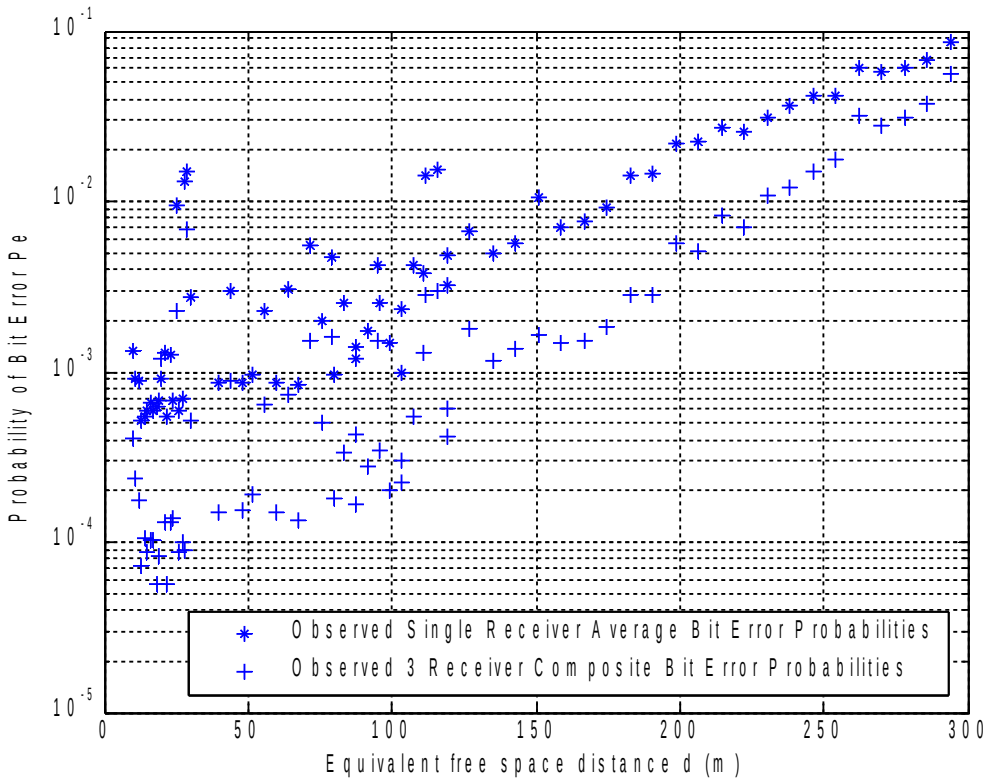

Fig 14: Observed Bit Error Probabilities for 3 Receiver Composite Case and Single Receiver Average

Section 2: Analysis of Short Range Effects:

Figs 11 and 12 imply that the system loss factor is not a constant; and that shorter distances yield a higher system loss factor. To examine this, the received bit energy to noise density per bit can be solved for for each point, allowing the received bit energy to be computed for each observed bit error reading. This may lend some insight into the short range effects of this receiver. Solving (6) and (7) for E_b/N_0 yields:

$$Q^{-1}(P_{e,FSK,coherent})^2 = \frac{E_b}{N_0} \tag{31}$$

$$-2*\ln(2*P_{e,FSK,noncoherent}) = \frac{E_b}{N_0} \tag{32}$$

The received energy, in these cases, appears to be approximately linear with respect to distance for distances greater than 70m. This would tend to imply that there is an upper statistical limit to the bit energy ratio that the receiver can accept, beyond which no benefit is gained.

Section 3: Inclusion of the Two Receiver Hybrid Case:

As a follow on discussion to the three receiver case, it becomes desirable to examine the benefits incurred as the receiver count increases progressively, ideally to quantify the benefits gained as a function of receiver number. By averaging the three two-receiver probabilities, a averaged two-receiver performance plot can be developed, with each of the three receivers being weighted exactly twice. However, since the each of the three pairs of receivers is not identical, the same analysis techniques used for the single receiver case and the three receiver composite case cannot be applied with the same confidence as to the one and three receiver cases. Specifically, the receiver #1 and receiver #3 pair are not identical to the receiver #1 and receiver #2 , and the receiver #2 and receiver #3 pairs. This is a known limitation to the two receiver case.

Section 4: Illustration of Probability Envelope and Correlation:

To show the degree of correlation between receivers, an envelope calculation is shown below. This illustrates that the different receivers on the board are highly correlated, as is to be expected from the proximity of the antennas together and the RF modules sharing a common ground plane. Figs 15 and 16 illustrate the expected probability envelopes for the three and two receiver cases, respectively. If the receivers were perfectly correlated, then the expected result would be that the multiple receiver cases would match perfectly with the single receiver case. If the receivers were statistically independent then the expected result would be an error probability based on the exponential of the receiver number.

As it is, the multiple receiver cases are highly, though not completely correlated with the single receiver case. This indicates that the multiple receivers do not perform in a constant gain format, but rather providing the most significant improvement at near field distances, where the level of the irreducible error for the composite receiver is less than that of the single receiver case.

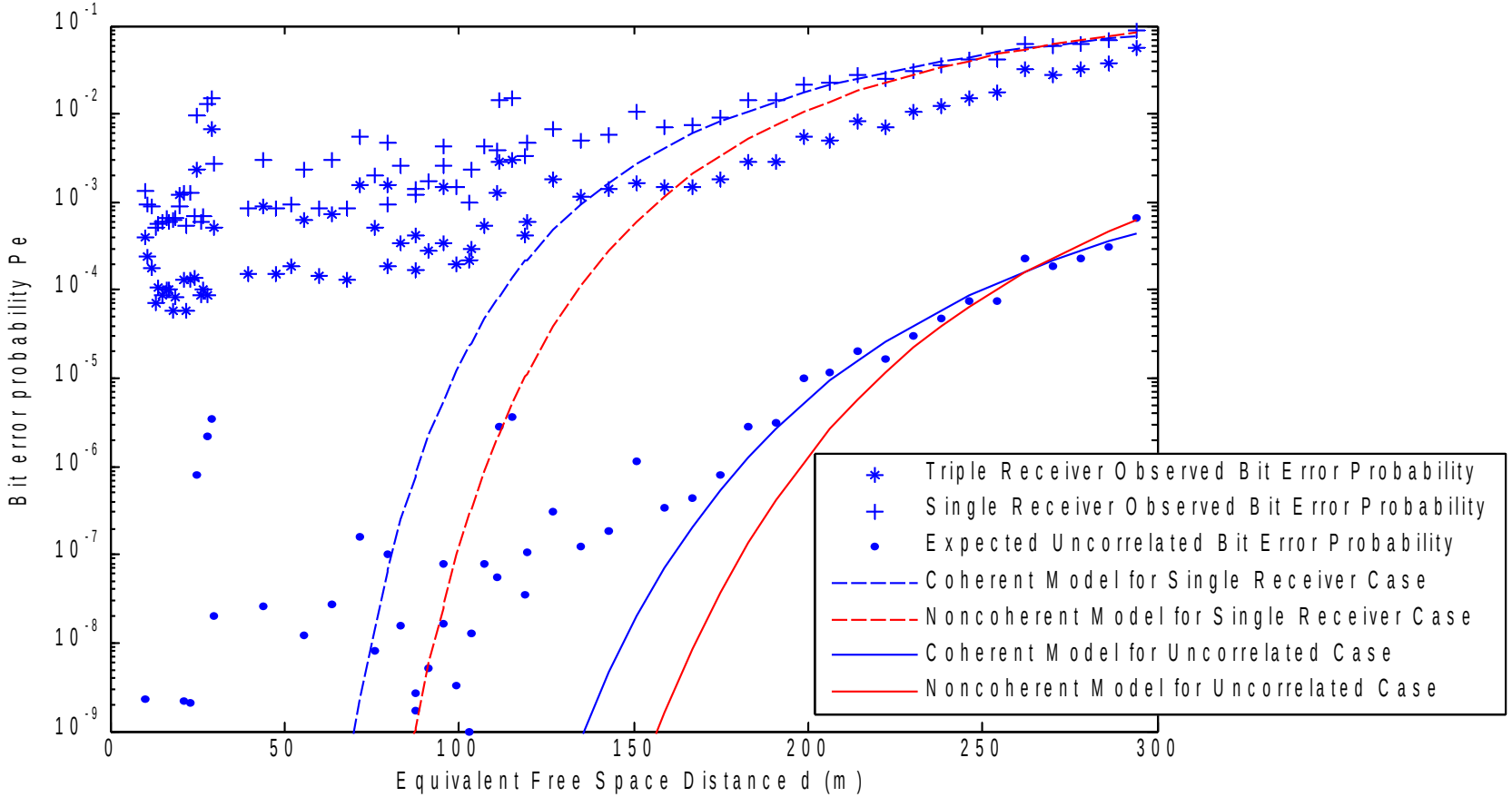

Fig 15: Triple Receiver Bit Error Probability Envelope

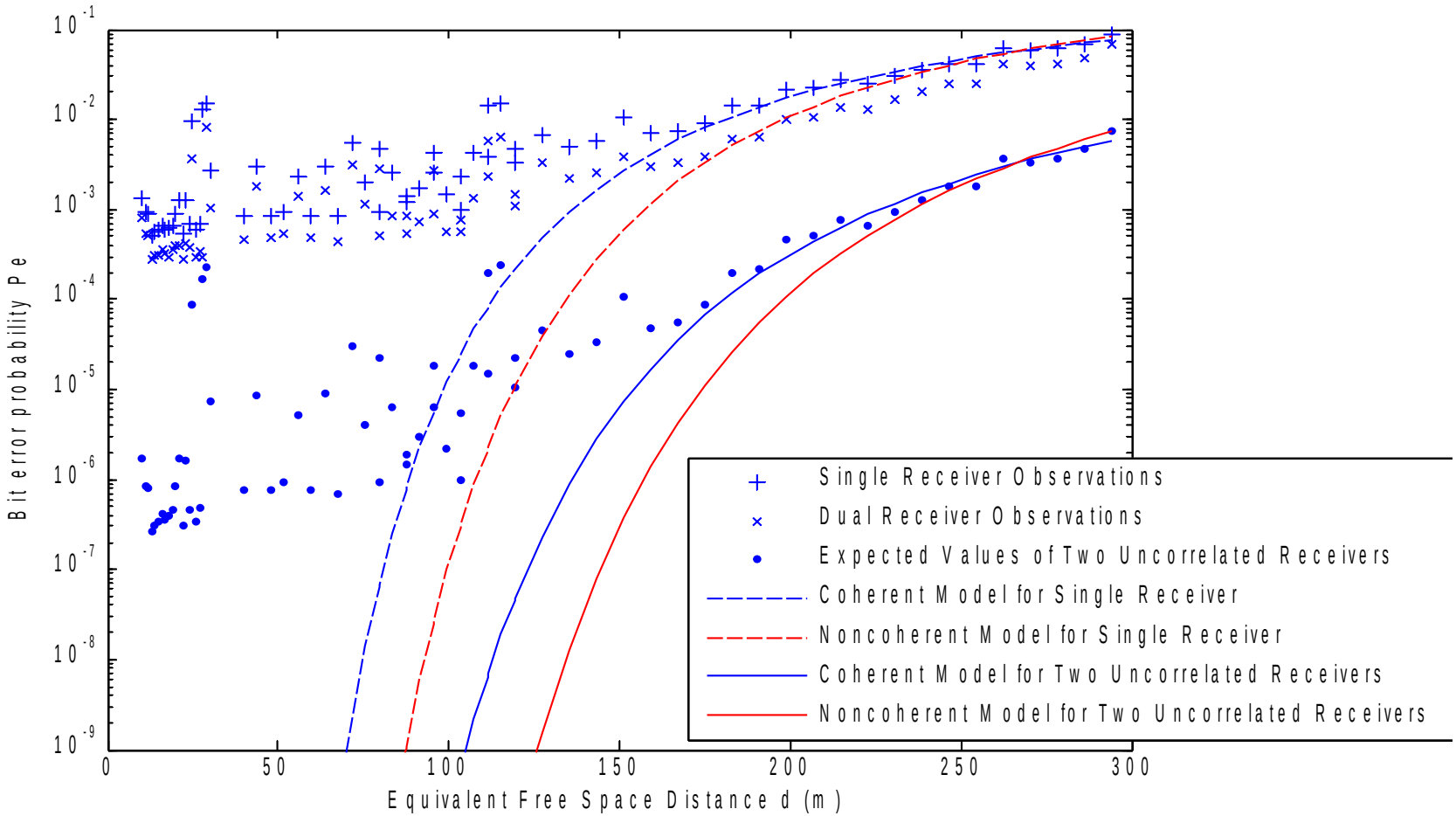

Fig 16: Two Receiver Bit Error Probability Envelope

Chapter 7: Summary and Conclusions

As telemetry and wireless sensing technologies advance, it becomes desirable to monitor previously inaccessible regions of many systems. This leads to the problem that wires often will not serve to extract data from the test section, whether that section is in a moving artillery shell, enclosed within a tire, or mounted on a high speed turbine blade.

All radio systems have a common set of problems associated with them. Signal degradation, power limitations, and interference all limit the ability of a receiver to perform. Standard methods of improving receiver performance include increasing the received signal to noise ratio with improved antennas, amplifiers and increasing the radiated power.

This thesis examined a single case of an alternative approach. Instead of increasing the received power, multiple receive units were used on a single test board, working in tandem to receive the data. The NRF24L01 single chip RF solution by Nordic Semiconductor was selected because of its high bit rate, low current consumption and small package size. The test board utilized three receivers sharing a common SPI bus and microcontroller. Testing involves sending pseudo-random data enumerating GF65521 over progressively longer distances. The structure of GF65521 was used to reconstruct packets and detect missing data. The lost packet turned out to be the dominant error mode of this particular chip, and analysis and modeling used a converted bit error rate based on the packet format. The estimated bit error rate appeared to improve by a factor of 10 at short distances, with this improvement being reduced as distance increased.

The three receiver composite did exhibit a performance improvement over that of the single receivers, but did so in a fashion that did not provide a gain in the same way an amplifier does. The chip has a minimum packet error rate, and therefore a minimum bit error rate, that applies regardless of received signal strength. The primary advantage of using multiple receivers appears to be that the redundancy causes this minimum bit error rate to drop significantly. At higher bit error rates, this effect is reduced, but generally the bit error rates where this occurs are sufficiently high that reliable communication is difficult.

Additionally, the chip has the option of using a CRC to detect corrupted data. The

testing performed as a part of this thesis demonstrated that turning the CRC off only increased the number of received packets by approximately 10%. Even within this 10% however, bit errors within the payload were not evenly distributed, indicating that a software error correction scheme of reasonable complexity could not recover all of the lost data. In this case, using the CRC built into the transmitter allows for minimum complexity and power consumption, with only a moderate cost in system performance. At free space distances of less than 100m, the improvement from one receiver to three receivers working in tandem more than offset this loss effect.

List of References

References:

[1] American Standard, Michelin, "Michelin IVTM brochure" [online document], 2005 [cited, 2007, Apr 25], Available HTTP: http://www.michelintruck.com/assets/pdf/IVTM.pdf

[2] American Trucking Associations, Inc., "Equipment and Maintenance Update", Transport Topics, February/March 2003 issue

[3] Michelin Technical Bulletin, "Michelin Etire HD Sensor Handling" [online document], June 15, 2006 [cited, 2007, Apr 25], Available HTTP: http://www.michelintruck.com/assets/pdf/bulletins/TB_etireHDSensor.pdf

[4] Michelin Press Release, "MICHELIN INNOVATION IN TIRE ELECTRONICS" [online document], Jan 4, 2004 [cited, 2007, Apr 25], Available HTTP: http://www.michelinman.com/difference/releases/pressrelease01042004g.html

[5] Sensicast corporate website, [online document], Mar 16, 2007, [cited, 2007, Apr 25], Available HTTP: http://www.sensicast.com/products.php,

[6] Specification of the Bluetooth System, "Version 2.0 + EDR" [online document], 4 November, 2004 [cited, 2007, Apr 25], Available HTTP: http://www.bluetooth.com/NR/rdonlyres/1F6469BA-6AE7-42B6-B5A1-65148B9DB238/840/Core_v210_EDR.zip

[7] IEEE, "Standard for Information Technology 802.15.4 Standard" [online document], 2006 [cited, 2007, Apr 25], Available HTTP: http://standards.ieee.org/getieee802/download/802.15.4-2006.pdf

[8] ZigBee Alliance, “ZigBee Specification 1.0,” [online document] June, 2005 [cited, 2007, Apr 25], Available by Request, HTTP: http://www.zigbee.org/en/spec_download/download_request.asp

[9] IEEE, “Standard for Information Technology 802.11G amendment” [online document], 2003 [cited, 2007, Apr 25] , Available HTTP: http://standards.ieee.org/getieee802/download/802.11g-2003.pdf

[10] National Security Agency, Network Hardware Analysis and Evaluation Division, “Recommended 802.11 Wireless Local Area Network Architecture” [online document], 1332-008R-2005, 9/23/2005 [cited, 2007, Apr 25], Available HTTP: http://www.nsa.gov/snac/wireless/I332-008R-2005.pdf

[11] M-G. Di Benedetto and G. Giancola, Understanding Ultra Wide Band Radio Fundamentals, Upper Saddle River, NJ: Prentice-Hall PTR, 2004.

[12] NSA Information Assurance Division, “Suite B Cryptography Fact Sheet” [online document, [cited, 2007, Apr 25], Quantico, Virginia, Available HTTP: http://www.nsa.gov/ia/industry/crypto_suite_b.cfm

[13] Nordic Semiconductor, “NRF24L01 datasheet” [online document], 2006, (rev 1.0 final), [cited, 2007, Apr 25] Oslo, Norway, Available HTTP: www.nordicsemi.com

[14] Analog Devices, “ADUC7019/20/21/22/24/25/26/27/28 datasheet” [online document], Apr, 2007, [cited, 2007, Apr 25] , Norwood, MA, Available HTTP: http://www.analog.com/UploadedFiles/Data_Sheets/ADUC7019_7020_7021_7022_7024_7025_7026_7027_7028.pdf

[15] Future Technology Devices International Ltd, “FT245R datasheet” [online document], 2005, [cited, 2007, Apr 25], Available HTTP: http://www.ftdichip.com/Documents/DataSheets/DS_FT245R.pdf

[16] Future Technology Devices International Ltd, “FT232R datasheet” [online document], 2005, [cited, 2007, Apr 25], Available HTTP: http://www.ftdichip.com/Documents/DataSheets/DS_FT232R.pdf

[17] Blahut, Richard E, Algebraic Codes for Data Transmission, second edition, Cambridge University Press, 2004

[18] Jon Gunnar Sponås, Nordic Semiconductors, personal communication, 12/5/2006

[19] Walpole, Myers, Myers, Ye, Probability and Statistics for Scientists and Engineers, seventh edition, Prentice Hall, 2002

[20] Rappaport, Theodore S, Wireless Communications, Principles and Practice, second edition, Prentice Hall, 2002

[21] Ziemer, Rodger E, Tranter, William H; Principles of Communications, Systems, Modulation, and Noise, fifth edition, John Wiley & Sons, 2002

Appendix

Table A-1: Experimental Results with a Power Setting of -18 dBm

Distance (m)	Total Sample Space	Ratio of Packets Missed by 3 Receivers	Ratio of Total Dropped Packets to Possible Receptions
10	2.2538E+04	3.7448E-02	1.148E-01
11	2.2615E+04	3.8382E-02	1.178E-01
12	4.5165E+04	1.6384E-02	1.150E-01
13	2.3853E+04	3.8737E-02	1.153E-01
14	2.2616E+04	3.8115E-02	1.162E-01
15	2.9932E+04	3.6550E-02	1.140E-01
16	2.4295E+04	3.6839E-02	1.131E-01
17	2.6828E+04	3.9064E-02	1.233E-01
18	3.5560E+04	3.9004E-02	1.265E-01
19	2.4060E+04	4.1355E-02	1.466E-01
20	2.6307E+04	4.6261E-02	2.002E-01
21	2.6693E+04	4.7054E-02	2.153E-01
22	2.7165E+04	5.6507E-02	2.571E-01
23	3.1536E+04	8.7297E-02	3.655E-01
24	3.3030E+04	8.6104E-02	3.764E-01
25	4.2210E+04	1.6520E-01	5.020E-01
26	4.9101E+04	1.4979E-01	5.172E-01
27	6.1254E+04	2.3332E-01	5.888E-01
28	6.2462E+04	2.0135E-01	5.632E-01
29	1.0924E+05	2.9174E-01	6.348E-01
30	7.1150E+04	3.2381E-01	6.914E-01
31	7.9250E+04	3.8257E-01	7.479E-01
32	7.8567E+04	4.3019E-01	7.473E-01
33	1.4011E+05	6.4184E-01	8.674E-01
34	8.0606E+04	5.9513E-01	8.498E-01
35	1.0648E+05	6.3943E-01	8.670E-01
36	4.2333E+04	7.0829E-01	8.950E-01
37	1.6643E+05	8.4198E-01	9.458E-01

Table A-2: Experimental Results with a Power Setting of -12 dBm

Distance (m)	Total Sample Space	Ratio of Packets Missed by 3 Receivers	Ratio of Total Dropped Packets to Possible Receptions
10	2.1126E+04	4.7808E-03	2.730E-02
11	5.3076E+04	2.8111E-02	9.048E-02
12	2.1938E+04	4.8774E-03	2.746E-02
13	2.8832E+04	6.0350E-03	3.022E-02
14	4.1892E+04	2.0052E-02	7.101E-02
15	2.0974E+04	4.7201E-03	2.734E-02
16	4.8479E+04	2.3495E-02	9.269E-02
17	2.1194E+04	4.2937E-03	2.647E-02
18	1.1344E+05	4.7435E-02	1.607E-01
19	3.8760E+04	1.6125E-02	6.227E-02
20	2.2249E+04	5.8430E-03	3.032E-02
21	1.6354E+04	1.0701E-02	7.764E-02
22	1.7246E+04	5.3926E-03	3.230E-02
23	1.6511E+04	8.7820E-03	5.390E-02
24	1.5789E+04	1.0957E-02	7.816E-02
25	2.8468E+04	6.3931E-03	4.660E-02
26	1.7911E+04	9.4914E-03	7.197E-02
27	3.2456E+04	1.7193E-02	1.280E-01
28	3.5309E+04	8.5389E-02	3.647E-01
29	2.1573E+04	9.0205E-02	3.905E-01
30	3.0248E+04	1.9340E-02	1.419E-01

Table A-3: Experimental Results with a Power Setting of 0 dBm

Distance (m)	Total Sample Space	Ratio of Packets Missed by 3 Receivers	Ratio of Total Dropped Packets to Possible Receptions
10	1.0775E+04	4.114E-02	4.114E-02
11	1.2133E+04	2.898E-02	2.898E-02
12	1.1928E+04	2.806E-02	2.806E-02
13	1.2566E+04	1.639E-02	1.639E-02
14	1.1175E+04	1.754E-02	1.754E-02
15	1.0154E+04	1.868E-02	1.868E-02
16	1.0339E+04	2.063E-02	2.063E-02
17	1.2673E+04	1.899E-02	1.899E-02
18	1.1461E+04	1.992E-02	1.992E-02
19	1.0681E+04	2.128E-02	2.128E-02
20	1.3020E+04	3.513E-02	3.513E-02
21	1.0923E+04	4.074E-02	4.074E-02
22	1.0346E+04	1.753E-02	1.753E-02
23	1.1570E+04	3.973E-02	3.973E-02
24	1.0726E+04	2.147E-02	2.147E-02
25	1.4361E+04	2.601E-01	2.601E-01
26	1.0521E+04	1.863E-02	1.863E-02
27	1.0202E+04	2.183E-02	2.183E-02
28	7.3430E+03	1.752E-02	1.752E-02
29	1.0813E+04	3.845E-01	3.845E-01
30	4.9670E+03	8.348E-02	8.348E-02

Vita

Thomas Ebel was born on July 10, 1983. He was raised in Natick, Massachusetts, attending the St Paul parochial school in Wellesley MA. He attended Boston College High School in Dorchester MA, graduating in 2001. From there, he attended St Louis University Parks College of Engineering, (now Parks College of Engineering, Aviation, and Technology), graduating with honors in 2005. He went on to complete a MS degree at the University of Tennessee Space Institute in Electrical Engineering.

Thomas is currently working as a project engineer in the avionics branch at Redstone Arsenal for the US DOD.